Indian Journal of Radio & Space Physics
Vol. 36, June 2007, pp. 219-228

Directional reflectance of vegetation targets: Simulation of its space measurements by coupling atmospheric and biophysical radiative transfer models

M R Pandya, R P Singh & S Panigrahy

Agriculture Forestry and Environment Group, Space Applications Centre, ISRO, Ahmedabad 380 015, Gujarat, India

E Mail: mrpandya@sac.isro.gov.in

Received 3 August 2006; accepted 7 March 2007

Vegetative surfaces are non-lambertian and deriving their spectral properties from space-borne sensors becomes complicated when off-nadir view angles are taken into consideration. In order to utilize off-nadir observations a complete understanding of directional reflectance is needed. This requires understanding of propagation of solar radiation as radiative transfer (RT) problem through a coupled system of vegetation canopy and atmosphere as a function of view angles. In this paper, a new approach of coupling biophysical (PROSAIL) and atmospheric (6S-code) RT models has been proposed to simulate at-sensor directional reflectance for vegetation target. At-sensor reflectance was simulated using 6S-code for the viewing geometry pertaining to 0, 5 and 26 deg view angles (hypothetical multispectral sensor with forward and backward viewing capabilities) for varying atmospheric conditions with the lower boundary condition parameterized through vegetation canopy reflectance obtained from PROSAIL model. Sensitivity of directional reflectance to input parameters were inferred at top-of-canopy and top-of-atmosphere level. The degree of anisotropy in reflectance pattern due to directional viewing represented by a parameter called g-factor was quantified (3-24% in red, 2-9% in near-infrared and panchromatic channels at top-of-atmosphere) which depends on wavelength and increases with atmospheric turbidity. This modeling study would help understanding capabilities of future space-borne sensors with directional/multi-spectral imaging.

Keywords: Directional reflectance, Non-lambertian surface, Biophysical radiative transfer, Atmospheric radiative transfer, Indian remote sensing (IRS) satellite
PACS No: 68.49. h; 78.40. q

1 Introduction

Vegetative surfaces scatter incident radiation anisotropically and therefore are called non-lambertian surfaces. Surface anisotropy is usually described in terms of bidirectional reflectance distribution functions (BRDF). These functions formally describe the scattering anisotropy of a certain type of surface dependent on wavelength (λ), illumination (sun zenith angle θ_s, sun azimuth angle ϕ_s) and viewing (view zenith angle θ_v, view azimuth angle ϕ_v) directions. Thus such functions actually depict the relationship between the incoming irradiance and the radiance reflected or scattered by a surface. The expression defining BRDF functions (f_r) is[1, 2]

$$f_r(\theta_S,\varphi_S;\theta_V,\varphi_V;\lambda) = \frac{dL_r(\theta_S,\varphi_S;\theta_V,\varphi_V;\lambda)}{dE_S(\theta_S,\varphi_S;\lambda)} \quad \ldots (1)$$

where, $dE_S = L_S.\cos\theta_S.d\omega_S = L_S.\cos\theta_S.\sin\theta_S d\theta_S d\varphi_S$ is the differential incident irradiance, L_s the incident radiance, dL_r the differential outgoing radiance. This definition ignores polarization, time variation, frequency shift and surface position dependence to reduce complexity. The BRDF has four important and interesting properties of non-negativity, Helmholtz reciprocity, energy conservation and isotropy[1].

A proper estimate and understanding of bidirectional reflectance or off-nadir reflectance is necessary[3] for land surface studies to carry out the following:

(i) Normalize the bidirectional effects in vegetation indices and reflectance data acquired under variable view angle conditions[4-5]
(ii) Use the directional signature for the estimate of surface parameter such as leaf area index (LAI), fraction of absorbed photosynthetic active radiation (fAPAR), albedo[6-9] and atmospheric parameter such as aerosol optical thickness (AOT)[10]
(iii) Classify land surface cover[11-12]
(iv) Evaluate the coupling between surface reflectance and atmospheric scattering for proper atmospheric correction[13]

Many Earth observation sensors (Table 1) are designed with off-nadir viewing capabilities by means

Table 1 — Some of Earth observation sensors with off-nadir viewing capabilities

Satellite-sensor	Spectral band	Spatial resolution	Viewing capability	Data acquisition technique
MISR	Blue, Green, Red, NIR	250 m	Nadir, ±(26.1, 45.6, 60.0, 70.5) deg	Nadir, Fore & Aft looking cameras, Along-track view
ASTER	VNIR	15 m	Nadir, -24 deg	Nadir & Aft looking telescopes, Along-track view
	SWIR	30 m	--	--
	TIR	90 m	--	--
POLDER	Blue, Green, Red, NIR	6km × 7km	±43 deg along track ±51 deg across track ±57deg diagonal FOV	CCD matrix detector with rotating wheels carrying polarizers and filters
MOMS-02	Blue, Green, Red, NIR	13.5 m	--	--
	Panchromatic		--	--
			Nadir, ±21.4 deg	Nadir, Fore & Aft looking telescopes, Along-track view
ATSR-1/2, AATSR	Green, Red, NIR, SWIR, 3.7,10.8,12 μm	1 km	Nadir, 55 deg	Nadir & Fore looking radiometer, Along-track view
IRS-1C/1D PAN	Panchromatic	5.8 m	±26 deg	Roll steering, Across-track view
IRS-1C/1D WiFS	Red, NIR	188 m	±26 deg	Large FOV/overlapping swaths, Across-track view
IRS-P6 Resourcesat- AWiFS	Green, Red, NIR, SWIR	56 m	±26 deg	Overlapping swaths, Across-track view
IRS-P6 Resourcesat-LISS-IV	Green, Red, NIR	5.8 m	±26 deg	Roll steering, Across-track view
IRS-P5 Cartosat FORE, AFT	Panchromatic	2.5 m	-5, 26 deg	Fore & Aft looking cameras, Along-track view

of large field of view or multi-angle imaging facility (AVHRR, SPOT, MODIS, POLDER, MISR, MOMS-02, WiFS, AWiFS, CARTOSAT, etc.). To utilize the data from such sensors to their fullest potential, a complete understanding of the off-nadir reflectance especially for vegetation targets is needed. This can be achieved by realistic simulation study involving the directional observational capability of the sensor.

Signals received by sensors aboard satellites in the optical wavelength region contain information about vegetative surface and the atmosphere, but in a coupled manner. The signal from actual surface, which is of interest, becomes more complicated when off-nadir viewing is considered. It is very important to differentiate between signal and perturbations introduced by the atmosphere and those effects that originate within the vegetative canopy. This certainly requires understanding of the propagation of solar radiation as radiative transfer (RT) problem through a coupled system of atmosphere and vegetation canopy.

The atmosphere and canopy components are solved independently, where atmospheric RT models alone are utilized to understand atmospheric effects on the surface remote sensing data[13-15] and these models generally require surface reflectance as a lower boundary condition, either by modeling or by measurements. Canopy RT models on the other hand are used to simulate the top of canopy (TOC) level vegetation reflectance to infer the influence of external factors such as viewing geometry[16-18]. Sufficient efforts have however not been made to bring TOC reflectance to the top of atmosphere (TOA) or at-sensor level, which is very vital, since atmosphere modulates the signal significantly. A coupling approach where atmosphere and canopy are used in attached mode is required, but scanty efforts have been made to couple canopy reflectance and atmospheric RT models, especially in Indian remote sensing (IRS) perspective. This becomes vital since Cartosat-1, which is an advanced IRS satellite has got an off-nadir viewing capability by forward and aftward looking cameras (Table 1) in panchromatic (PAN) band with a very fine spatial resolution of 2.5 m. Before using the data available from such unique sensor-configuration, role of directional reflectance needs to be understood through modeling studies.

In this paper, results on a study to simulate at-sensor directional reflectance from vegetative surfaces using coupled biophysical (PROSAIL) and atmospheric (6S-code) RT model have been reported

for an existing and a hypothetical Indian remote sensing sensor with viewing capability of 0°, 5° and 26° in panchromatic (PAN), red and near infrared (NIR) spectral channels.

2 Methodology

The methodology adopted for this study has been described in the following three subsections: (i) the concept of coupling atmosphere and canopy components, (ii) detailed description of models used in the study and (iii) simulation of at-sensor directional reflectance from vegetation surface using coupled model. The simulation of at-sensor observations is carried out by taking into account the effects related to the IRS sensor characteristics (spectral bands and resolution), atmospheric variations and the angular sun-target-sensor configuration.

2.1 The concept of coupling atmosphere and canopy

The classic approach of using decoupled atmospheric or canopy RT has been used extensively in the past [Fig. 1(a), (b)] for remote sensing of vegetative surfaces from spaceborne sensors, to understand the effects introduced by the atmosphere or vegetative canopy. As indicated in Fig. 1(a), in the atmospheric modeling component, the canopy is represented as the bottom boundary condition (BC). This requires data of BRDF, of plant canopy of interest, which may be obtained either from canopy modeling calculations or from measurements. However, in the canopy modeling component [Fig. 1(b)], the atmospheric effects must be included in the specification of the upper canopy boundary conditions which, in principle, presumes the solution of the atmospheric RT problem [Fig. 1(a)] either by modeling or measurement. This problem of specifying the correct boundary conditions at atmosphere-canopy interface is eliminated when a coupled system of atmosphere and canopy [Fig. 1(c)] is considered for the analysis.

The detailed problem formulation of coupled (atmospheric and vegetation) system, ideally requires the solution of the RT equation and a system description in terms of all possible interaction processes of solar radiation with given system components. However, a complete systems description in terms of differential scattering and absorption cross-sections is difficult and complicated due to the large number of systems components and their variable nature. So, an approach of solving atmospheric and canopy RT has been proposed and used in this study to simulate at-sensor directional reflectance in red, NIR and panchromatic (PAN) wavelength regions for vegetation target using canopy and atmospheric RT models.

2.2 Model description

At the moment, several canopy reflectance models are available; some of them simulate the anisotropy of canopy reflectance, particularly the hotspot effect, with greater accuracy. Some other models are better suited either for sparse or dense canopies[19]. In order to model the spectral reflectance of a plant canopy the PROSAIL model is chosen, while to simulate satellite level signal 6S RT code is selected. This is because it is a physically based model that is not optimized to one specific satellite sensor, scene or site. Moreover it is fully documented, and is well suited for various applications.

2.2.1 The PROSAIL model

The PROSAIL is a combination of two radiative transfer models, PROSPECT[20] that simulates leaf spectral properties and SAIL[13] that describes canopy

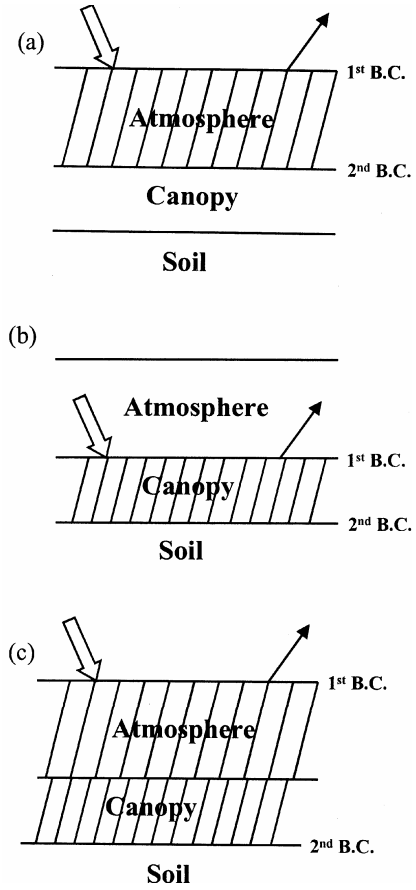

Fig. 1 — Schematic showing modeling of (a) Atmospheric RT, (b) Canopy RT and (c) Coupled Atmosphere-Canopy RT

reflectance. The PROSPECT simulates the leaf optical properties, from the visible (400 nm) to middle infrared (2500 nm), as a function of three variables: a parameter that accounts for the internal structure of the leaf mesophyll (N), a chlorophyll a+b concentration expressed in μg cm^{-2} (C_{ab}) and a water depth expressed in cm (C_w). Scattering from arbitrarily inclined leaves[16] (SAIL) is a one-layer RT based canopy reflectance model, which simulates near-realistic plant canopy bidirectional reflectance. As described by Verhoef[16], SAIL model is a modified version of an analytical canopy reflectance model proposed by Suits[21]. The Suits model is an extension of the so-called AGR model of Allen, Gayle and Richardson[22], which, in turn, is an extension of the Duntley equations that are, in turn, extensions of the Kubelka-Munk theory[16] of light scattering and extinction in diffusing media in general. The SAIL model in essence is four-flux theory involving a diffuse downward flux E_-, a diffuse upward flux E_+, a direct solar flux E_s and flux associated with the radiance in the direction of observation (E_o). The system of four differential equations involving four flux (Fig. 2) and nine coefficients is as follows:

$$\frac{dE_S}{dx} = kE_S \quad \ldots (2a)$$

$$\frac{dE_-}{dx} = -sE_S + aE_- - \sigma E_+ \quad \ldots (2b)$$

$$\frac{dE_+}{dx} = s'E_S - aE_+ + \sigma E_- \quad \ldots (2c)$$

$$\frac{dE_0}{dx} = wE_s + vE_- + uE_+ - KE_0 \quad \ldots (2d)$$

where, x represents the vertical dimension of canopy layer, while k, K, a are extinction coefficients and s, s', σ, u, v, w are scattering coefficients. The method of solutions of system [Eq. (2)] has been discussed elsewhere[22]. Expressions of the nine extinction and scattering coefficients that depend on viewing geometry are presented in the following set of equations.

$$k(\theta_1) = \frac{2}{\pi}L'\left[\beta_s - \frac{\pi}{2}\cos\theta_1 + \sin\beta_s\tan\theta_s\sin\theta_1\right]$$

where, $\beta_s = \cos^{-1}\left(\frac{-1}{\tan\theta_s\tan\theta_1}\right)$ and $L' = \frac{L}{h}$,

h=thickness of layer, L=LAI

$$K(\theta_1) = \frac{2}{\pi}L'\left[\beta_o - \frac{\pi}{2}\cos\theta_1 + \sin\beta_o\tan\theta_o\sin\theta_1\right]$$

$$\beta_o = \cos^{-1}\left(\frac{-1}{\tan\theta_o\tan\theta_1}\right)$$

$$\sigma(\theta_1) = L'\left[\frac{\rho+\tau}{2} + \frac{\rho-\tau}{2}\cos^2\theta_1\right]$$

$$\sigma'(\theta_1) = L'\left[\frac{\rho+\tau}{2} - \frac{\rho-\tau}{2}\cos^2\theta_1\right]$$

$$s(\theta_1) = \frac{\rho+\tau}{2}k(\theta_1) - \frac{\rho-\tau}{2}L'\cos^2\theta_1$$

$$s'(\theta_1) = \frac{\rho+\tau}{2}k(\theta_1) + \frac{\rho-\tau}{2}L'\cos^2\theta_1$$

$$u(\theta_1) = \frac{\rho+\tau}{2}K(\theta_1) - \frac{\rho-\tau}{2}L'\cos^2\theta_1$$

$$v(\theta_1) = \frac{\rho+\tau}{2}K(\theta_1) + \frac{\rho-\tau}{2}L'\cos^2\theta_1$$

$$w(\theta_1) = \frac{L'}{2\pi}\left\{\begin{aligned}&[\pi\rho - \beta_2(\rho+\tau)]\\ &\times\left(2\cos^2\theta_1 + \sin^2\theta_1\tan\theta_s\tan\theta_0\cos\psi\right)\\ &+(\rho+\tau)\sin\beta_2\left[\frac{2\cos^2\theta_1}{\cos\beta_s\cos\beta_0}\right.\\ &\left.+\cos\beta_1\cos\beta_3\sin^2\theta_1\tan\theta_s\tan\theta_0\right]\end{aligned}\right\}$$

where, auxiliary azimuth angles β_1, β_2 and β_3 are determined from a decision table depending upon β_s and β_0.

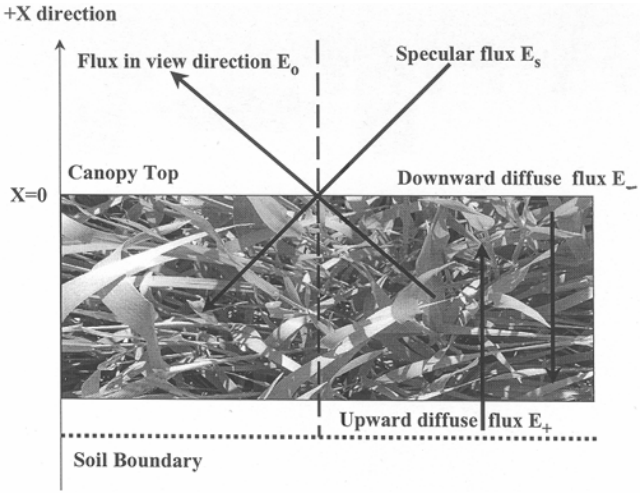

Fig. 2 — Schematic of canopy reflectance model showing direction of four fluxes in SAIL model

$$a(\theta_1) = \kappa(\theta_1) - \sigma'(\theta_1)$$

where, $\kappa = L'$ and σ' is diffuse forward scattering coefficient

$$\text{Therefore, } a(\theta_1) = L'\left[1 - \frac{\rho + \tau}{2} + \frac{\rho - \tau}{2}\cos^2\theta_1\right]$$

The parameters occurring in SAIL model are, the leaf reflectance (ρ_l) or transmittance (τ_l), leaf area index (LAI), average leaf inclination angle (θ_l), soil reflectance (ρ_s), fraction of diffused incident solar radiation (skyl) and parameters describing measurement conditions (solar zenith θ_s and azimuth ϕ_s angles, view zenith θ_v and azimuth angles ϕ_v). Among these parameters, four (ρ_l, τ_l, ρ_s and skyl) are wavelength dependent. In summary, the canopy spectral reflectance calculated by PROSAIL model depends on, biophysical parameters: C_{ab}, C_w, N, LAI and θ_l; soil spectral reflectance, $\rho_s(\lambda)$ which will be assumed known; and external parameters: θ_s, ϕ_s, θ_v, ϕ_v and skyl.

2.2.2 6S-code (Second simulation of the satellite signal in the solar spectrum)

Satellite sensors measure the radiance reflected from the Earth's surface. However, radiance is distorted by various factors in the path of Sun-target-sensor. Molecular scattering, gaseous absorption and aerosols affect the TOA signal measured by the instrument. Due to the effect of the atmosphere, only a fraction of photons (80% at 0.85 μm and 50% at 0.45 μm) coming from the target reach the sensor[13]. So there is a difference between radiation received by the satellite and radiation reflected from the surface target. The missing photons are lost through absorption and scattering. The absorption is mainly caused by O_3, H_2O, O_2, CO_2, CH_4 and N_2O, while ash, dust and aerosols in the atmosphere cause the scattering. In order to quantitatively obtain accurate information about the target, these atmospheric distortions should be removed by some radiative transfer process. The best way is to simulate the RT process through analytical code, considering the variable constituents that influence the signal measured by the satellite. The 6S radiative transfer code is used for this purpose.

As described in the work of Vermote[13], target reflectance at the satellite level is sum of five terms [Fig. 3]: (1) the photons directly transmitted from the Sun to the target and directly reflected back to the sensor; (2) the photons directly transmitted to the target but scattered by the atmosphere on their way to the sensor; (3) the photons scattered by the atmosphere and reaching to the sensor; (4) the photons scattered by the atmosphere then reflected by the target and directly transmitted to the sensor; and (5) photons reaching the sensor reflected by neighboring regions. Here the focus is not to describe each step considered in 6S code, which is quite complicated. The problem is simplified and following modality [Eq. (3)] of the 6S code is used to represent the radiance received by the satellite at the TOA for heterogeneous surface.

Suppose $\rho_{TOA}(\theta_s, \theta_v, \phi)$ is the reflective radiation received at the sensor at the top of the atmosphere (TOA) from the target with reflectivity ρ. Then it is expressed as[13]

$$\rho_{TOA}(\theta_s,\theta_v,\varphi) = t_g(\theta_s,\theta_v)\left\{\rho_a(\theta_s,\theta_v,\varphi) + \frac{T(\theta_s)}{1-\rho_e S} \times\left[\rho e^{-\frac{\tau}{\mu_v}} + \rho_e t_d(\theta_v)\right]\right\} \quad \ldots (3)$$

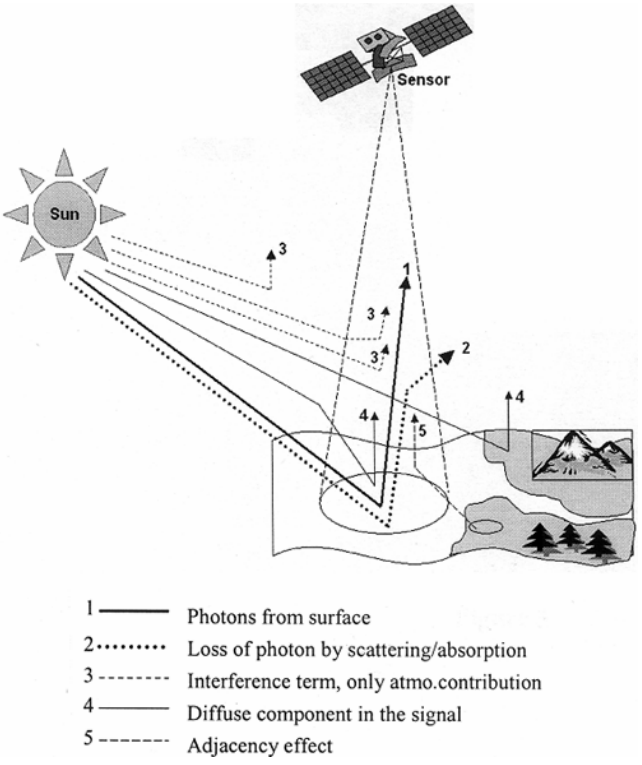

Fig. 3 — Schematic representation of radiative flux components considered in the atmospheric RT model

where

$\rho_a(\theta_s, \theta_v, \phi)$ = intrinsic reflectance of the molecular and aerosol scattering,

S = spherical albedo of the atmosphere

θ_s, θ_v, ϕ are solar zenith, view zenith and relative azimuth angles

ρ = target reflectance

ρ_e= background/environment reflectance

$T(\theta_s)$ = total downward atmospheric transmission

$T(\theta_v)$ = total upward atmospheric transmission

$T_g(\theta_s, \theta_v)$ = transmission factor for aerosol and water vapour absorption

The transmission terms T can be divided into the two parts: direct radiation transmittance and diffuse transmittance factor, given by

$$T(\theta_s) = e^{-\frac{\tau}{\mu_s}} + t_d(\theta_s) \text{ and}$$

$$T(\theta_v) = e^{-\frac{\tau}{\mu_v}} + t_d(\theta_v)$$

where, $t_d(\theta_s)$ represents downward diffuse transmittance factor and $t_d(\theta_v)$ the upward transmittance factor; $e^{-\frac{\tau}{\mu_s}}$ and $e^{-\frac{\tau}{\mu_v}}$ the transmittance of the radiation directly transmitted to the surface and the radiation reflected directly to the sensor, respectively. Here, $\mu_s = \cos\theta_s$ and $\mu_v = \cos\theta_v$ are the cosine of the sun and satellite zenith angle respectively, and τ the optical thickness of the atmosphere.

Summarizing, the inputs to 6S code are as follows: geometric conditions (day/month of satellite pass, sun zenith, sun azimuth, view zenith and view azimuth angles); atmospheric water and ozone contents; selective aerosol model; aerosol optical depth at 550 nm; spectral channel; target and sensor altitude; and reflectance of the target.

2.3 Simulation set-up to generate at-sensor directional reflectance

In this study, PROSAIL model was used (described in Sec 2.2.1) to compute canopy reflectance for all possible range of its input parameters[23]. The range of input parameters used in PROSAIL model is summarized in Table 2. The directional reflectance at TOC was simulated for these inputs as a function of satellite view zenith angle (θ_v: 0, 5, 10, 15, 20, 25, 26, 30, 35, 40, 45, 50, 55, 60 deg) and solar zenith angle (θ_s: 53 deg). The view zenith angle range considered in this experiment corresponds to the viewing capability of various missions like AWiFS, MODIS, NOAA and Cartosat. Solar zenith and azimuth considered in this study were using values corresponding to IRS-P6 pass over Bareja site[24] (72º 38′ E, 22º 52′ N) of 28 Nov. 2003. All the simulations were carried out for red (0.62-0.68 μm), NIR (0.77-0.86 μm) and PAN (0.50-0.85 μm) spectral regions pertaining to IRS sensors spectral resolution. By simulating canopy reflectance using PROSAIL, major aspects related to optical observation of vegetation and realistic modeling of directional reflectance was covered. However, this still gives only the reflectance, as it would have been measured on the ground, not what a sensor would observe from space. Therefore, the coupling of the surface reflectance model to an atmospheric RT model has been devised as shown in Fig. 4.

The canopy reflectance (top of canopy) simulated from PROSAIL model was then used as lower boundary conditions to the 6S-code, and at-sensor reflectance was simulated for the viewing geometry pertaining to 0º, 5º and 26º view angles (hypothetical IRS multispectral sensor with forward and backward viewing capabilities). Using the inputs listed in Table 3, atmospheric simulations were performed for varying atmospheric conditions, keeping water vapour and ozone content constant, and varying aerosol

Table 2 — Range of variation used for each input variable of PROSAIL RT model[23]

Model Variable	Symbol	Units	Minimum	Maximum	Average
Leaf area index	LAI	-	1.0	6.0	3.0
Leaf inclination	θ_l	deg	25	65	45
Leaf internal structure	N	-	1.25	2.0	1.5
Leaf chlorophyll a+b content	C_{ab}	μg cm^{-2}	22	52	32
Leaf equivalent water thickness	C_w	cm	0.01	0.04	0.0255
Solar zenith angle	θ_s	deg	53	53	53
View zenith angle*	θ_v	deg	0	60	5° interval

* View zenith angle used: 0°-60° at 5° interval with 26° as a special case

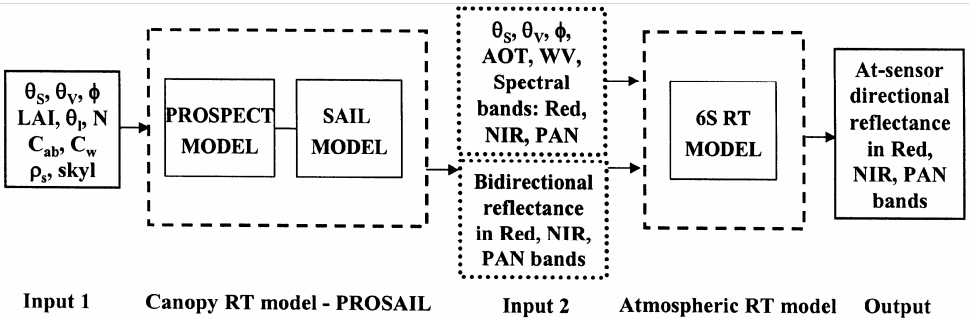

Fig. 4 — Simulation set-up for coupling models with input/output parameters

Table 3 — 6S code input parameters used in study[24]

Satellite/sensor parameters	
Spectral channels	IRS LISS-III Red, NIR
	IRS Cartosat-PAN
Spectral resolution, μm	0.62-0.68 (IRS LISS-III Red)
	0.77-0.86 (IRS LISS-III NIR)
	0.50-0.85 (IRS Cartosat-PAN)
Altitude, km	820 (IRS LISS-III)
	623 (IRS Cartosat-PAN)
Viewing geometry	
Day/ Month	28/ November
Sun Zenith Angle	53 deg
Sun Azimuth Angle	161 deg
View Zenith Angle	0, 5, 26 deg
View Azimuth Angle	0 deg
Atmospheric conditions	
Water vapour, g cm^{-2}	1.64
O_3 content, cm-atm	0.30
Aerosol model	Continental
AOT at 550 nm	0.10, 0.25, 0.50, 0.75

optical thickness (AOT) by 0.1 (clear), 0.25 (average), 0.50 (turbid) and 0.75 (very turbid). Anisotropic factor (hereafter called g-factor), which is defined as the ratio of off-nadir reflectance to nadir reflectance, was quantified for all simulation results at TOC (pertaining to all view angles between 0 and 60 deg) and at TOA for selected cases (pertaining to view angles of 0º, 5º and 26º).

3 Results

3.1 Directional reflectance and g-factor at TOC

The influence of each of the canopy parameters (chlorophyll content, LAI, water content, leaf inclination angle, leaf internal structure) on the directional reflectance was studied by simulating the TOC reflectance by PROSAIL model as a function of view zenith angle ranging between 0 and 60 deg. The relative influence of each of the canopy parameters was assessed by keeping other canopy parameters

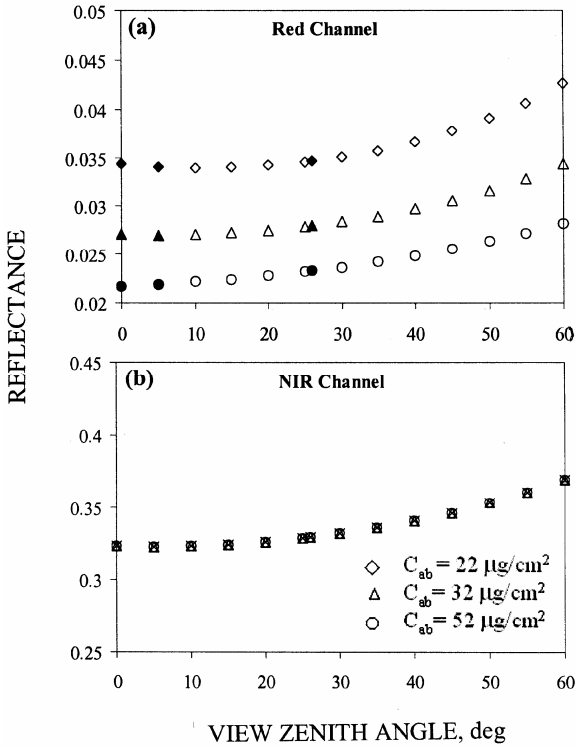

Fig. 5 — Directional reflectance in (a) red and (b) NIR channels as a function of view zenith angle for different leaf chlorophyll content

constant at their representative average value[23] (C_{ab} = 32 μg cm^{-2}, LAI = 3, C_w = 0.0255 cm, θ_l = 45º, N = 1.5). The directional reflectance in red and NIR wavelength on TOC for varying chlorophyll contents are shown in Figs 5(a) and (b), while Figs 6(a) and (b) show the graphs for varying LAI. Similar graphs were prepared for PAN bands and for other canopy parameters (not shown).

Figure 5 illustrates the dependence of canopy reflectance on view angles for varying C_{ab}. As expected, chlorophyll a+b absorbs light in the red band and this absorption domain is completely different for the NIR region. As chlorophyll content

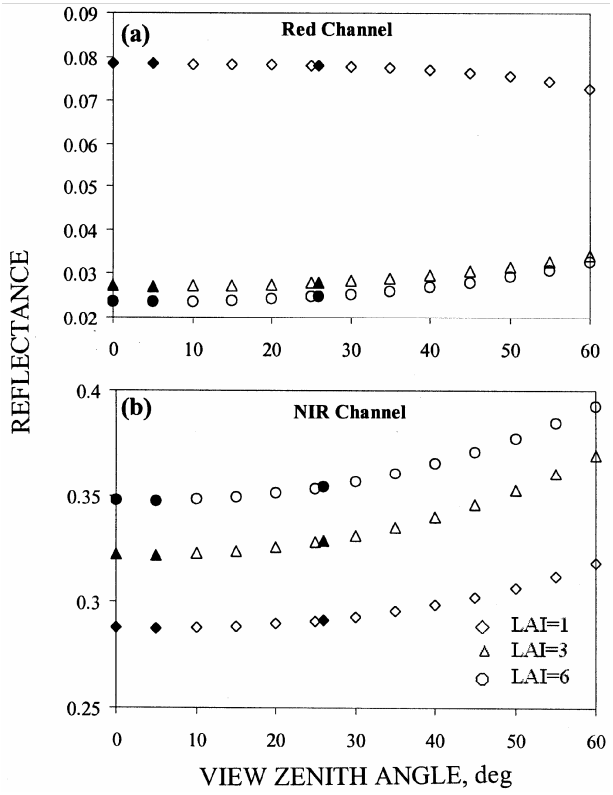

Fig. 6 — Directional reflectance in (a) red and (b) NIR channels as a function of view zenith angle for different leaf area index

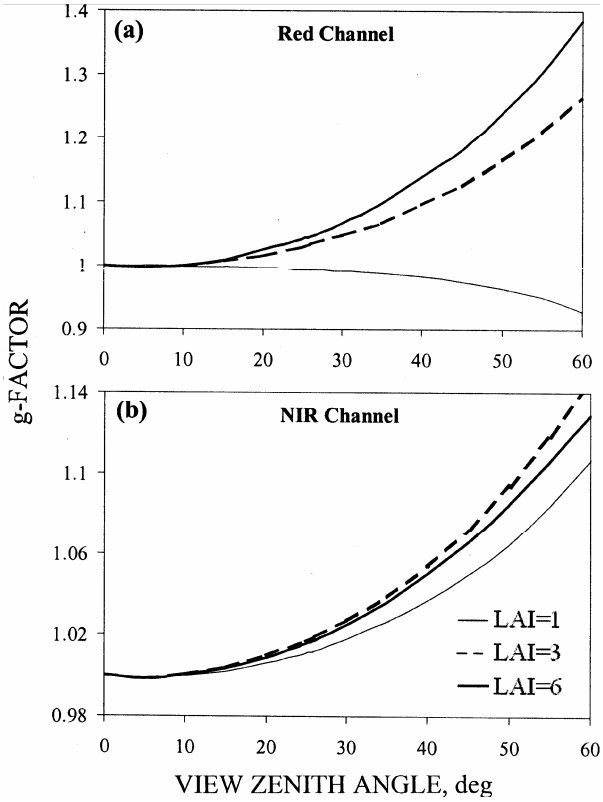

Fig. 7 — At-TOC anisotropic factor (g-factor) in (a) red and (b) NIR channels as a function of view zenith angle for different leaf area index

increases red reflectance decreases, which is obvious since for less chlorophyll content leaves would have a tendency of stress condition and thus absorption would be less, so that red reflectance shows higher values. Red reflectance decreases with increase in chlorophyll content, since absorption increases. While reflectance in NIR region is not governed by the absorption by chlorophyll pigments, so it remains same for varying chlorophyll content. The reflectance in both the wavelength regions shows increase with increasing view angle (approximately 24% in red and 14% in NIR reflectance) except in red region for very sparse vegetation (LAI = 1). Figure 6 illustrates the dependence of canopy reflectance on view angles for varying LAI. As LAI increases red reflectance decreases and NIR increases. Since reflectance in NIR portion of the spectrum is predominantly governed by the scattering from the leaf layers and so for higher LAI, NIR reflectance would be high. The filled symbols in Figs 5 and 6 represent the view angle position for 0º, 5º and 26º, showing possible variation corresponding to existing IRS forward and backward viewing angles.

The g-factor that represents the anisotropy of the directional reflectance introduced due to the variation in view angle at TOC for red and NIR channels for varying LAI conditions is shown in Figs 7(a) and (b). Similar graphs were prepared for other inputs also (not shown). The off-nadir reflectances are greater than nadir reflectance, so the g-factor shows smooth increasing trend except for LAI = 1 case for red channel. The variation in g-factor is about 38% for red channel and 14% for NIR channel.

3.2 Directional reflectance and g-factor at TOA

Out of all the results, the simulated TOA directional reflectance of red channel is shown for varying atmospheric conditions, represented by varying AOT for vegetation surface with LAI 1 and 6 in Figs 8(a) and (b), respectively. It shows how atmosphere adds the reflectance for red region. And the contribution of atmosphere increases with increase in off-nadir view angles. So such atmospheric effects have to be considered before using the off-nadir data. The g-factor for TOA observations for LAI 1 and 6 in red channel are shown in Figs 9(a) and (b). It shows a variation of 15% and 23% for LAI 1 and 4 respectively, while for NIR channel it showed 5-6%. Overall a possible variation of 3-24% in red and 2-9%

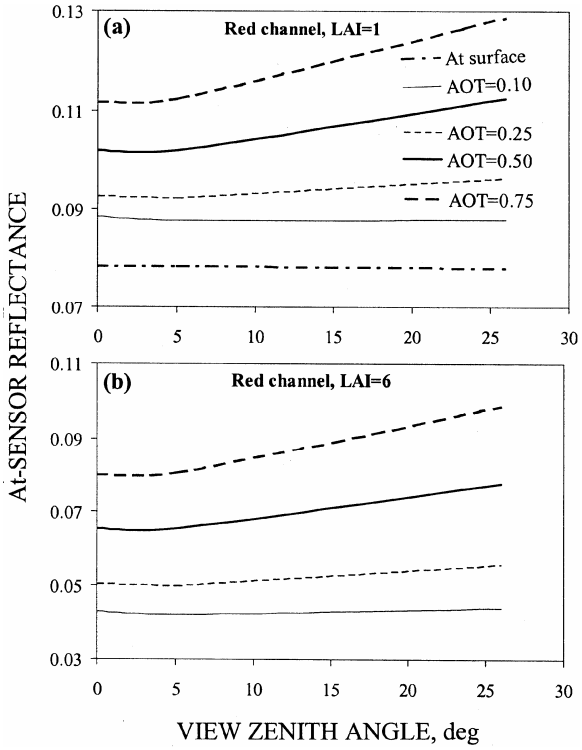

Fig. 8 — Directional reflectance in red channel for (a) LAI = 1 and (b) LAI = 6 as a function of view zenith angle for different AOT

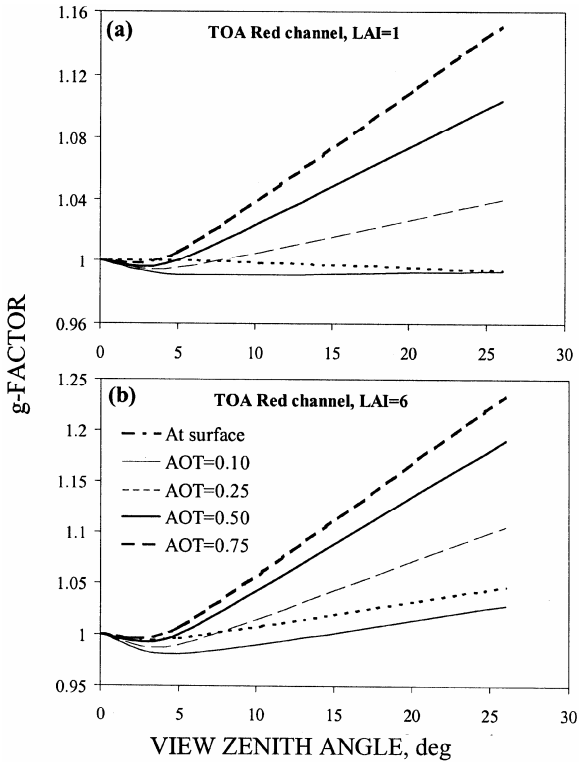

Fig. 9 — At-TOA anisotropic factor (g-factor) for (a) LAI = 1 and (b) LAI = 6 as a function of view zenith angle for different AOT in red channel

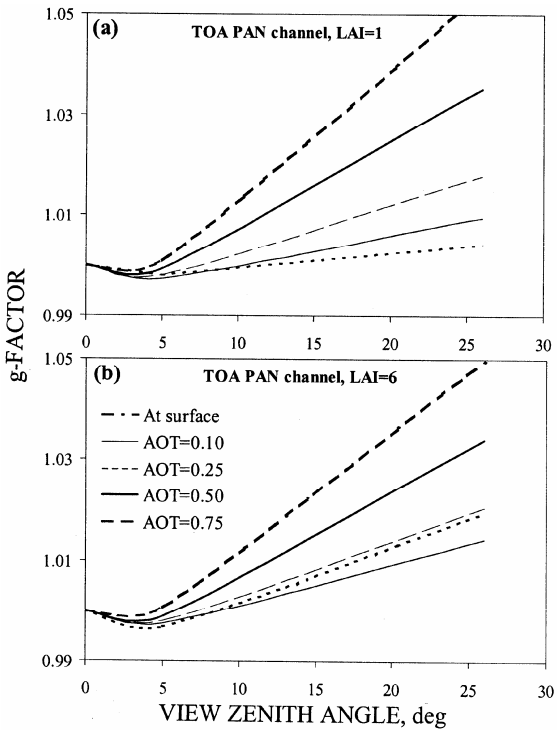

Fig. 10 — At-TOA anisotropic factor (g-factor) for (a) LAI = 1 and (b) LAI = 6 as a function of view zenith angle for different AOT in PAN channel

in NIR channels were observed for all the input parameters. A variation of 2-9% was observed in the case of PAN channel as shown in Figs 10(a) and (b). Once this kind of anisotropic factor is quantified it could be useful in normalizing the off-nadir and nadir data as well as in the hemispherical integration, which is common in radiance to flux conversion in energy budgeting calculation using broad band sensors.

4 Conclusions

In this paper a study on coupling biophysical (PROSAIL) and atmospheric (6S-code) RT models have been described for space measurements. This coupling approach was used to simulate directional reflectance and surface anisotropy effect for a hypothetical space borne sensor with forward and backward viewing capabilities for vegetation canopy having different biophysical characteristics in varying atmospheric conditions. The analysis was carried out for red, NIR and panchromatic regions of the spectrum. The understanding and quantification of anisotropic factor (g-factor) carried out in the study would be useful in deriving nadir to off-nadir convertibility. It would also be a useful quantity while taking the hemispherical integration for all the view angles in radiance to flux conversion for broad band

sensors. This study provides a new approach of coupling biophysical and atmospheric RT models, which simulates at-sensor directional reflectances in IRS spectral bands. It provides an appreciation of responses of vegetation target for directional viewing, which would facilitate in understanding future sensors with directional and multi-spectral imaging capabilities.

Acknowledgements

Authors gratefully thank Dr. R R Navalgund, Director, Space Applications Centre, Dr. J S Parihar, Group Director, Agriculture Forestry and Environment Group, SAC for their guidance and support during the course of this study.

References

1 Claustres L, Boucher Y & Paulin M, Wavelet-based modeling of spectral bidirectional reflectance distribution data, *Opt Eng (USA)*, 43 (2004) 2327.

2 Kukko A, Yyyppä J & Kuittinen R, Use of HRSC-A for sampling bidirectional reflectance, *ISPRS J Photogram Remote Sens (UK),* 59 (2005) 323.

3 Maignan F, Bréon F M & Lacaze R, Bidirectional reflectance of Earth targets: evaluation of analytical models using a large set of spaceborne measurements with emphasis on the hotspot, *Remote Sens Environ (USA),* 90 (2004) 210.

4 Leroy M & Roujean J L, Sun and view angle corrections on reflectances derived from NOAA/AVHRR data, *IEEE Trans Geosci Remote Sensing (USA),* 32 (1994) 684.

5 Wu A, Li Z & Cihlar J, Effects of land cover type and greenness on advanced very high radiometer bidirectional reflectances: analysis and removal, *J Geophys Res (USA),* 100 (1995) 9179.

6 Knyazikhin Y, Martonchik J V, Diner D J, Myneni R B, Verstraete M M, Pinty B & Gobron N, Estimation of vegetation canopy leaf area index and fraction of absorbed photosynthetically active radiation from atmosphere-corrected MISR data, *J Geophys Res (USA),* 103 (1998) 32239.

7 Bicheron P & Leroy M, A method of biophysical parameter retrieval at global scale by inversion of a vegetation reflectance model, *Remote Sens Environ (USA),* 67 (1999) 251.

8 Wanner W, Strahler A H, Ju B, Lewis P, Muller J P, Li X, Schaaf C L B & Barnsley M J, Global retrieval of bidirectional reflectance and albedo over land from EOS MODIS and MISR data: theory and algorithm, *J Geophys Res (USA),* 102 (1997) 17143.

9 Cabot F & Dedieu G, Surface albedo from space: coupling bidirectional models and remotely sensed measurements, *J Geophys Res (USA),* 102 (1997) 19645.

10 Diner D J, Beckert J C, Reilly T H, Bruegge C J, Conel J E, Kahn R A, Martonchik J V, Ackerman T P, Davies R, Gerstl S A W, Gordon H R, Muller J-P, Myneni R B, Sellers P J, Pinty B & Verstraete M M, Multi-angle imaging spectroradiometer (MISR) instrument description and experiment overview, *IEEE Trans Geosci Remote Sens (USA),* 36 (1998) 1072.

11 Hyman A H & Barnsley M J, On the potential for land cover mapping from multiple view angle (MVA) remotely sensed information, *Int J Remote Sens (UK),* 18 (1997) 2471.

12 Zhang Y, Tian Y, Myneni R B, Knyazikhin Y & Woodcock C E, Assessing the information content of multiangle satellite data for mapping biomes: I. Statistical analysis, *Remote Sens Environ (USA),* 80 (2002) 418.

13 Vermote E F, Tanfe D, Deuzé J L, Herman M & Morcrette J-J, Second simulation of the satellite signal in the solar spectrum, 6S: An overview, *IEEE Trans Geosci Remote Sens (USA),* 35 (1997) 675.

14 Staenz K, Williams D T, Fedosejevs G & Teillet P M, Surface reflectance retrieval from Imaging Spectrometer Data using three atmospheric codes, *Proc. EUROPTA* '94, Strasbourg, France, 1994.

15 Teillet P M & Santer R P, Terrain elevation and sensor altitude dependence in a semi-analytical atmospheric code, *Can J Remote Sens (Canada),* 17 (1991) 36.

16 Verhoef W, Light scattering by leaf layers with application to canopy reflectance modeling: the SAIL model, *Remote Sens Environ (USA),* 16 (1984) 125.

17 Pandya M R & Dadhwal V K, Simulation of top of canopy red and nir crop reflectance for proposed INSAT-2E CCD payload using SAIL model, *Proc. of ISRS-Symposium*, Bangalore, 19-21 Dec., 1999, 63.

18 Pandya M R, Dadhwal V K & Navalgund R R, Effect of WiFS viewing geometry on crop reflectance: a simulation study using SAIL model, *Int J Remote Sens (UK),* 21 (2000) 1931.

19 Goel N S, Models of vegetation canopy reflectance and their use in estimation of biophysical parameters from reflectance data, *Remote Sens Review (USA),* 1 (1987) 221.

20 Jacquemoud S & Baret F, PROSPECT: a model of leaf optical properties spectra, *Remote Sens Environ (USA),* 34 (1990) 75.

21 Suits G H, The calculation of the directional reflectance of a vegetative canopy, *Remote Sens Environ (USA),* 2 (1972) 117.

22 Allen W A, Gayle T V & Richardson A J, Plant canopy irradiance specified by the Duntley equations, *J Opt Soc Am (USA),* 60 (1970) 372.

23 Jacquemoud S, Inversion of PROSPECT+SAIL canopy reflectance model from AVIRIS equivalent spectra: theoretical study, *Remote Sens Environ (USA),* 44 (1993) 281.

24 Pandya M R, Singh R P, Chaudhari K N, Oza S R, Bairagi G D, Dadhwal V K & Parihar J S, *Spectral and radiometric evaluation of sensors onboard IRS-P6*, Scientific Report SAC/RESIPA/SR-02/Oct 2004.